Extrapolation of Proton Electromagnetic Form Factor*

J. S. LEVINGER† AND RONALD F. PEIERLS‡
Cornell University, Ithaca, New York
(Received 13 January 1964)

We use the assumed analytic properties of the proton electromagnetic form factors $G(t)$ by performing a conformal transformation to a new variable η such that the form factor is analytic inside the unit circle in the complex η plane. We fit the data with power series in η and extrapolate to the circle to find the spectral function. For both electric and magnetic form factors, we find spectral functions with a broad peak around 625 MeV, and a negative excursion above 1 BeV. We examine the validity of our extrapolation procedure by tests on several types of artificial data. Our procedure can reproduce a spectral function with a broad peak, but is not so successful in reproducing a narrow resonance, or a pair of narrow resonances close together.

I. INTRODUCTION

NUCLEON electromagnetic form factors[1] are generally believed to be analytic functions of the variable t, the negative squared four-momentum transfer, in the entire t plane except for a cut from some (positive) t_0 to infinity. The physically accessible region for electron-scattering experiments is t real and nonpositive. (See Fig. 1.) The form factor $G(t)$ in the physical region, which is real,[2] can be expressed as an integral along the cut involving the discontinuity in $g(t)$ across the cut (or in other words the imaginary part g of G just above the cut):

$$G(t)=\frac{1}{\pi}\int_{t_0}^{\infty}\frac{g(t')dt'}{t'-t}+G(-\infty). \quad (1)$$

We use a subtracted dispersion relation: $G(-\infty)$ is the subtraction constant. We wish to use measured form factors $G(t)$ in a finite part of the physical region to obtain the spectral function $g(t')$.

It is well known that Eq. (1) must be written four times: for the isovector and isoscalar portions of the electric and magnetic form factors, respectively. In this paper we limit ourselves to the use of measured proton form factors, since these measurements are at present much more accurate than those for the neutron. That is, we deal with the sum of isoscalar and isovector form factors in $G(t)$ and therefore the sum of isovector and isoscalar spectral functions $g(t')$. Physically, the spectral function is closely related to the mass spectrum of strongly interacting systems of spin 1^-, baryon number and strangeness zero and of appropriate isotopic spin. Thus, in the isovector case the lowest possible mass is $t_0=4\mu_\pi^2$, the threshold for two pions: The isoscalar system must have a mass of at least 3 pions and has $t_0=9\mu_\pi^2$.

We shall consider Eq. (1) for the electric and magnetic[3] form factors G_E and G_M for the proton, rather than the Dirac and Pauli form factors F_1 and F_2. A main reason for this choice is that for large values of t the magnetic form factor G_M is much more accurately determined by present data than are F_1 or F_2.

Many different workers have used measured form factors to determine the spectral functions: We shall review briefly a small part of this work. If we assume the spectral function to be sharply peaked, $g(t')$ can be approximated by a delta function at some resonance position t_R, giving a one-pole form for G. Data on $g(t')$, can be used to determine both the strength of the resonance and the value of t_R. Fubini,[4] and Hofstadter,[5] and Kirson[6] have found such fits to the data, but only if t_R is as low as $20\mu_\pi^2$, corresponding to a resonant mass of about 600 MeV. For example, using the experimental data for the proton magnetic form factor given in Table I, Kirson finds a statistically acceptable χ^2 value of 15.2, for 17 deg of freedom. Ball and Wong[7] have argued that this pole can be interpreted as the (isovector) ρ meson of mass 750 MeV, provided its width is taken into account. However, this argument does not apply to the corresponding isoscalar resonance, the ω

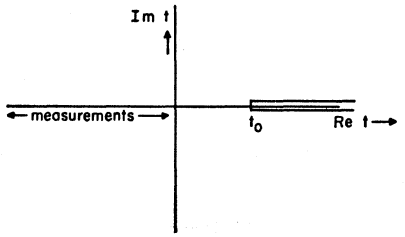

FIG. 1. The t plane for form factors. The physical region is four-momentum transfer t real and nonpositive. The t plane has a cut starting at positive real threshold t_0.

* Supported in part by the U. S. Office of Naval Research. Preliminary accounts were given Bull. Am. Phys. Soc. 8, 365 (1963), at the Cambridge Photon Conference (January 1963) and at the Stanford Conference on Nuclear Structure (June 1963).

† AVCO Visiting Professor.

‡ Present address: at Brookhaven National Laboratory.

[1] S. D. Drell and F. Zacharaisen, *Electromagnetic Structure of Nucleons* (Oxford University Press, London, 1961).

[2] In most discussions of the extrapolation of scattering amplitudes, the phase of the amplitude is not given directly by experiment, while in this case the scattering amplitude is real in the one-photon approximation.

[3] L. N. Hand, D. G. Miller, and R. Wilson, Rev. Mod. Phys. **35**, 335 (1963).

[4] S. Fubini, in *Nuclear and Nucleon Structure*, edited by R. Hofstadter (W. A. Benjamin and Company, Inc., New York, 1963), paper 79.

[5] C. deVries, R. Hofstadter, and R. Herman, in *Nuclear and Nucleon Structure*, edited by R. Hofstadter (W. A. Benjamin and Company, Inc., New York, 1963), paper 81.

[6] M. W. Kirson and J. S. Levinger, Bull. Am. Phys. Soc. **8**, 364 (1963) and M. W. Kirson (private communication).

[7] J. S. Ball and D. Y. Wong, Phys. Rev. **130**, 2112 (1963).

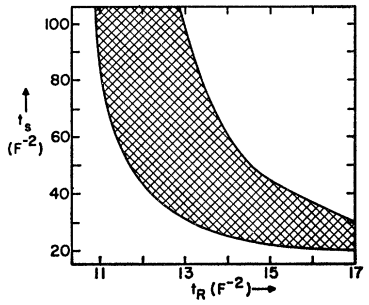

FIG. 2. The shaded region shows the region in the t_R-t_S plane giving statistically acceptable two-pole fits to the proton form factors. Here t_R and t_S are the positions of the two poles.

meson of mass 790 MeV and extremely narrow width. It therefore seems clear that a one-pole fit to current proton form-factor measurements is not satisfactory if we require consistency with other experimental evidence on the position of the pole.

Other workers[3,6,8] have introduced extra parameters into the proton's spectral function by assuming that it could be approximated by two poles. They find that a two-pole fit (with subtraction constants) can be achieved with reasonable positions for the two poles. One pole can be chosen at t_R near the ρ and ω resonances while a second can be chosen at t_s to represent the average behaviour of the proton's spectral function above 1 BeV. Kirson and Levinger[6] find a variety of fits to the data for G_E and G_M which are statistically acceptable, i.e., the hatched region shown in Fig. 2. The positions of the two poles cannot be determined from form-factor data alone. All the fits have the property that the coefficient of the pole in the 750-MeV region ($t_R=15F^{-2}$) is opposite in sign to the coefficient of the pole in the 1200-MeV region ($t_s=40F^{-2}$) but of the same general size. The combination of the two simulates a Clementel-Villi formula for one pole at a lower mass. Kirson[9] has made a fit of this type identifying the higher mass pole with the ϕ resonance (1020 MeV) and the lower mass one with a mixture of ρ and ω.

The problem of obtaining the spectral function $g(t')$ from the measured $G(t)$ is essentially that of using the analytical form of G [Eq. (1)] to extrapolate from the physical region ($t\leq 0$) to the region $t>t_0$. Most of the fits discussed above achieve this by assuming the extrapolated form to be a sum of delta functions and then fitting the parameters to the data. This has two drawbacks. First, the location of and behavior at the threshold is nowhere used in the choice of the extrapolated form, and therefore we are not using some available information. Secondly, the extrapolated form depends in a very nonlinear way on the parameters (positions and strengths of the poles) which introduces complications in the statistical fitting. Specifically, the parameters have to be introduced in pairs, with the result that while a one-pole fit may not be quite good enough, the two-pole fits involve one more parameter than the data can determine. Hence, there is a wide variety of such fits (see Fig. 2); and the number of parameters has to be reduced by requiring one pole to occur at the ρ mass, in order to tie down the fit.

In the present paper we make use of a different method of extrapolating which avoids both these difficulties, being linear in the parameters used and explicitly making use of the threshold behavior. The technique is to use a conformal transformation, discussed by many authors[10] which transforms the cut t plane to the interior of the unit circle. The transformed data are then fitted by a polynomial in the new variable whose coefficients can be used to extrapolate to the spectral function. The information about the location and nature of the threshold is used in the specification of the transformation (the extrapolated spectral function automatically vanishes below t_0), and also by an explicit constraint requiring the slope of $g(t')$ to vanish at t_0.

The results of this procedure seem to indicate that the proton form-factor spectral functions peak fairly sharply near the ρ mass and become negative at higher energies. This agrees very well with the conclusions of

TABLE I. Data used for proton magnetic form factor. Compilation of proton magnetic form factors G_M and their standard errors, as of February 1963. The relation between t and η is given in Eq. (2), using $b=2$, and $t_0=2.0F^{-2}$.

$q^2=-t$ in F^{-2}	η	G_M	Error	Ref.
0.0	0.333	2.793	0.000	static value
1.0	0.240	2.508	0.036	a, b
1.6	0.197	2.394	0.025	a
2.0	0.171	2.234	0.036	b
2.98	0.118	2.034	0.016	c
4.56	0.049	1.650	0.099	d
7.0	−0.029	1.370	0.360	d
9.0	−0.079	1.130	0.068	d
10.0	−0.101	1.120	0.045	e
11.5	−0.130	1.020	0.052	d
13.0	−0.156	0.930	0.056	d
15.0	−0.186	0.890	0.052	d
16.5	−0.206	0.730	0.023	d
18.0	−0.226	0.640	0.038	d
21.5	−0.263	0.540	0.022	d
25.0	−0.295	0.464	0.012	d, f
30.0	−0.333	0.382	0.014	f
35.0	−0.366	0.314	0.012	f
40.0	−0.393	0.232	0.018	f
45.0	−0.416	0.238	0.022	f

[a] D. J. Drickey and L. N. Hand, Phys. Rev. Letters **9**, 521 (1962).
[b] B. Dudelzak, G. Sauvage, and P. Lehmann, Nuovo Cimento **28**, 18 (1963). (We have not used the G_{MP} values quoted by these authors at $q^2=0.30F^{-2}$ and $q^2=0.49F^{-2}$.)
[c] P. Lehmann, R. Taylor, and R. Wilson, Phys. Rev. **126**, 1183 (1962).
[d] F. Bumiller, M. Croissiaux, E. Dally, and R. Hofstadter, Phys. Rev. **124**, 1623 (1961), as analyzed by M. W. Kirson and J. S. Levinger, Phys. Rev. **130**, 1549 (1963).
[e] T. J. Janssens, R. Hofstadter, E. B. Hughes, and M. R. Yearian, Bull. Am. Phys. Soc. **7**, 620 (1962).
[f] K. Berkelman, M. Feldman, R. M. Littauer, G. Rouse, and R. R. Wilson, Phys. Rev. **130**, 2061 (1963).

[8] S. Goto, Nuovo Cimento **27**, 1249 (1963).
[9] M. W. Kirson, Phys. Rev. **132**, 1249 (1963).

[10] W. R. Frazer, Phys. Rev. **123**, 2180 (1961); C. Lovelace, Nuovo Cimento **25**, 730 (1962); D. Atkinson, Phys. Rev. **128**, 1908 (1962); R. Theis, Cambridge Photon Conference, 1963 (unpublished), and private communication; J. D. L. Zeiler (private communication).

the two-pole fits, but it is encouraging that at no stage do we have to *require* any peaking near the ρ mass.

Section II contains details of the method of fitting and the constraints imposed. In Sec. III we apply these techniques to the data on the proton form factors G_E and G_M. Section IV is devoted to the question of the significance of our extrapolations. Most of our discussion is applicable to other problems; e.g., $\pi-p$ scattering. The statistical uncertainty is easily assessed, but in order to obtain some idea of the reliability of the method we construct artificial data from known spectral functions and study the results of extrapolating by the same technique. In the final section we discuss our results for the form-factor spectral functions and compare with other fits to the experimental data.

II. EXTRAPOLATION PROCEDURE

The measured form factors give values, for $t\leq 0$, of a function $G(t)$ whose analytic structure is given by Eq. (1). We introduce a new variable

$$\eta=[b-(1-t/t_0)^{1/2}]/[b+(1-t/t_0)^{1/2}], \qquad (2)$$

defining a conformal transformation[10] which, taking the appropriate branch of the square root, maps the entire t plane of Fig. 1 into the interior of the unit circle shown in Fig. 3. The cut from t_0 to $+\infty$ goes into the boundary of the unit circle, the upper semicircle corresponding to the upper branch of the cut. The origin goes into the point $(b-1)/(b+1)$ which by suitable real choice of b can be placed on the real η axis anywhere between -1 and $+1$. We therefore consider a new function $K(\eta)=G(t)$, which is analytic inside the unit circle, and can be expanded in a power series

$$K(\eta)=\sum_{n=0}^{\infty} a_n\eta^n. \qquad (3)$$

For real $t>t_0$ Eq. (2) can be written

$$\eta=\exp[i\xi(t)], \qquad (4)$$
$$\cos\xi=(b^2+1-t/t_0)/(b^2-1+t/t_0),$$

and hence

$$g(t)=\mathrm{Im}G(t)=\mathrm{Im}K[\exp(i\xi)]=\sum_{n=1}^{\infty} a_n \sin n\xi(t). \qquad (5)$$

Our procedure will be to assume that the power series (3) can be approximated by a few terms, determine their coefficients a_n which best fit the data and use these values in (5) to evaluate $g(t)$.

In discussing the validity of this procedure we have to be careful to formulate the information we are seeking. If we were to ask for a point by point quantitative evaluation of $g(t)$ two serious questions would arise. Firstly, there is the question of the convergence of the procedure even if we could determine an arbitrary number of coefficients a_n. This has been considered in a rather similar situation by Atkinson,[10] who concludes in fact that except at higher branch points the procedure should formally converge. Secondly, there is the question of the uncertainty introduced into the extrapolation by taking only a few terms of the series, which are all that can be determined from present data. It is fairly clear that, in fact, the error on any given point is liable to be quite large, and further, that the extrapolated value of g for any particular value of t may be sensitive to such things as the choice of the parameter b. However, we may ask a somewhat weaker question: Does the extrapolated function reproduce the main qualitative features of the true spectral function? The qualitative features in question are such things as dominance by a low-energy resonance or the lack thereof; change of sign of $g(t)$ in some energy region, etc. In order to answer this question we have taken a number of artificial known spectral functions; used Eq. (1) to calculate a series of values of $G(t)$ and then introduced random errors so as to simulate actual data. In Sec. IV we discuss the fits obtained with such "pseudodata." For the moment we remark merely that the results do seem to bear out the extrapolation procedure as a qualitative tool. Accordingly we do not need to consider further the thornier problems of convergence or uniqueness.

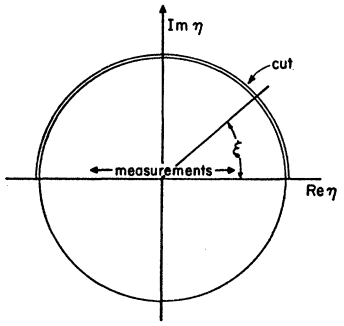

FIG. 3. The η plane for form factors. The physical region is along the real axis from -1 to $(b-1)/(b+1)$. The cut is along the upper semicircle; angle ξ is given in Eq. (4).

The data were fitted by trying to determine the first N coefficients of the power series. This is not necessary but is the most natural choice for two reasons. Firstly, these are the terms which are most important for small $|\eta|$, which is the experimental region. Secondly, the neglected higher terms correspond to rapidly oscillating components of the spectral function, which one can hope will not be so essential to its main qualitative behavior.

The parameter b was chosen for each set of data so as to spread the data points about equally on both sides of the origin in the η plane. This increases the total range of values of η while keeping the range of $|\eta|$ as small as possible, which provides the best determination of the fewest parameters. If b were chosen so as to make the data very asymmetric and require larger values of $|\eta|$, a reasonable statistical fit would require a larger number of coefficients but as these do not really imply more information their values would be highly correlated. Variation of b can greatly change the relation between the angle ξ and t: Although the final fit was made with

b chosen as indicated above, fits were aiso made with b varying to confirm that the general behavior of the spectral function remained the same.

The data were required to satisfy a linear constraint at $t=0$;

$$G_E(0)=\sum_{n=0}^{N} a_n{}^E[(b-1)/(b+1)]^n=1.0,$$
$$G_M(0)=\sum_{n=0}^{N} a_n{}^M[(b-1)/(b+1)]^n=2.793, \tag{6}$$

where $a_n{}^E$, $a_n{}^M$ are the coefficients for the electric and magnetic form factors, respectively. A second constraint was sometimes used: the requirement that the slope of $g(t)$ vanish at $t=t_0$ [the function $g(t)$ automatically vanishes there as is easily seen from Eqs. (4) and (5)]. The requirement of zero slope corresponds to the fact that there is a centrifugal barrier resisting the generation of 1^- states. This condition is easily expressed as

$$\sum_{n=1}^{\infty} na_n=0. \tag{7}$$

It is clearly not a rigorous procedure to apply this condition to the truncated series instead. Furthermore for the isoscalar part of the form factor t_0 is actually *below* threshold. However, the condition

$$\sum_{n=1}^{N} na_n=0, \tag{8}$$

while not the correct constraint, should help to ensure that the slope of the extrapolated function does not behave too erratically near $t=t_0$. Fits were made both with and without this constraint.

The fitting was carried out using standard least-squares methods, modified to allow the inclusion of the linear constraints (6) and (8). The modification is particularly simple in the case of linear constraints; as it does not seem to be generally known the details are given in the Appendix. The fits were made with an increasing number of parameters until the value of χ^2 stopped to improve. If the experimentally quoted errors are approximately Gaussian and are independent, then for a good fit χ^2 should be of the order of the number of degrees of freedom. As might have been expected from the two-pole fits, the data seem to determine three free parameters. These can be the coefficients of a cubic without the second constraint (8) or the coefficients of a quartic making use of the second constraint. In addition to watching the behavior of the χ^2, another check on the correct number of parameters can be obtained from the behavior of the error matrix. When too many parameters are used, the parameters are no longer well determined, and this excessive freedom shows up as a large statistical uncertainty or "error" on the extrapolated points. It should be emphasized that this is really the only significance which should be attached to these "errors"; they are definitely *not* estimates of the expected rms deviation from the true value of the spectral function.

III. FITS TO MAGNETIC AND ELECTRIC FORM FACTORS

We shall now apply the methods discussed in the previous sections. For the magnetic form factor of the proton, G_M, we use the 19 data points given in Table I. The magnetic form factors are given[11] in Table I to an accuracy of better than 5% for four-momentum transfer squared q^2 in the range $0\leq q^2\leq 35\text{F}^{-2}$, and to better than 10% accuracy for the two highest values of q^2.

The fits obtained by using these data tend to give very large values for the extrapolated value $G(t)$ at $t=-\infty$ ($\eta=-1$). In some cases, therefore, we have introduced a fictitious data point

$$G(-\infty)=0.0\pm 0.2G(0), \tag{9}$$

with fairly large error so as to prevent the extrapolated value from becoming too large. This can be regarded, on the one hand, as a check to make sure that the spectral function is not too sensitive to the behavior at physical but inaccessibly large momentum transfers, and on the other, as a search for possible evidence on the subtraction constant.

In discussing the results we shall refer to the fits as "free," "constrained," or "restricted." Free fits are those carried out subject only to the constraint (6) on the static form factors. Constrained fits are those subject in addition to the constraint (8) affecting the threshold behavior of the spectral function. Restricted fits are those in which the extra data point (9) has been used.

Recent measurements at high values of t support a restriction such as Eq. (9) on *both* G_M and G_E. The measurements[12] at the Cambridge linear accelerator show that both (real) form factors decrease with increasing q^2 in the range $45\leq q^2\leq 125\text{F}^{-2}$; there is no evidence for "cores" or subtraction constants. The experiment[13] on

TABLE II. Goodness of fit versus degree of polynomial. The χ^2 values are for the fits to the 19 values of G_M in Table I, fitted by polynomials in η of degree N; $\phi=\chi^2$/degrees of freedom.

	Free polynomial		Constrained		Constrained and restricted	
N	χ^2	ϕ	χ^2	ϕ	χ^2	ϕ
2	147	8.6	788	43.7	832	44
3	13.8	0.86	77.4	4.55	77.5	4.3
4	12.4	0.83	16.2	1.02	50.2	2.96
5	11.8	0.84	12.8	0.85	13.2	0.83
6	...	...	11.9	0.85	12.6	0.84

[11] We made an error of 0.7 standard errors in the datum for $q^2=15\text{F}^{-2}$; this should have quite a small effect on the fit.

[12] K. W. Chen, A. A. Cone, J. R. Dunning, S. G. F. Frank, N. F. Ramsey *et al.*, Phys. Rev. Letters **11**, 561 (1963).

[13] M. Conversi, Siena Conference on Elementary Particles, October 1963 (unpublished); M. Conversi, J. Massan, Th. Muller, and A. Zichichi, Phys. Letters **5**, 195 (1963); K. J. Barnes, Nuovo Cimento **28**, 284 (1963).

TABLE III. Coefficients for constrained fits to G_M. The coefficients a_n and diagonal errors Δa_n for constrained polynomials of degree N fitted to the G_M data of Table I.

	$N=4$		$N=5$		$N=6$	
n	a_n	Δa_n	a_n	Δa_n	a_n	Δa_n
0	1.555	0.012	1.532	0.017	1.517	0.024
1	4.180	0.049	4.320	0.091	4.279	0.100
2	−0.065	0.132	0.743	0.461	1.633	1.041
3	−4.885	0.410	−6.785	1.116	−4.943	2.232
4	2.651	0.339	−2.423	2.792	−11.00	9.42
5	...	...	4.848	2.648	−8.17	13.9
6	...	...	...	...	15.35	16.11

proton-antiproton annihilation into an electron-positron pair gives a preliminary upper bound on a linear combination of G_E^2 and G_M^2 in the time-like region $q^2<-90\text{F}^{-2}$, where the form factors can be complex. Our fits to the data of Table I are meant to *illustrate* our procedure of obtaining the spectral function from a given set of experimental data. In Sec. V we discuss work that will be of interest as further data becomes available.

Throughout this section we use the conformal transformation Eq. (2), for $b=2$, and threshold value $t_0=4\mu_\pi^2=2.0\text{F}^{-2}$.

In Table II we examine the values of χ^2 versus degree N of the polynomial in η used to fit the data of Table I. We also give the ratio

$$\phi=\chi^2/\text{degrees of freedom}. \tag{10}$$

This ratio ϕ should have a value near unity for a good fit. There are (19–N) degrees of freedom for the free polynomial, and (20–N) for the constrained polynomial.

We see from Table II that in each case χ^2 at first drops very rapidly with increasing N, and then levels off rather abruptly. For the free polynomial it is obvious that $N=3$ is the correct value to use for this type of fit to the data of Table I. For the constrained polynomial one might wonder whether $N=4$ or $N=5$ should be used, since the value of χ^2 drops from 16.2 to 12.8. We argue that $N=4$ should be used, since the value $\phi=1.02$ is already reasonable, and use of $N=5$ gives a large increase in the standard errors of the coefficients a_n. (See Table III.) For the constrained and restricted polynomial, it is clear that we should use $N=5$. We see that the data of Table I cover a large enough range and have sufficient accuracy to determine 3 adjustable parameters for the free cubic, or constrained quartic. Adding the restriction Eq. (9) for $G(-\infty)$ allows the determination of a fourth adjustable parameter. The fact that we can fit with ϕ near unity shows that the errors quoted in Table I are realistic.

TABLE IV. Coefficients for best fits to G_M. Coefficients a_n and diagonal errors Δa_n for different polynomial best fits in η to magnetic form factors of Table I.

	Free cubic		Constrained quartic		Constrained and restricted quintic	
n	a_n	Δa_n	a_n	Δa_n	a_n	Δa_n
0	1.545	0.011	1.555	0.012	1.540	0.012
1	4.235	0.055	4.180	0.049	4.278	0.061
2	0.334	0.102	−0.065	0.132	0.471	0.127
3	−5.418	0.469	−4.885	0.410	−6.198	0.578
4	...	...	2.651	0.339	−0.723	0.393
5	...	...	...	...	3.253	0.535

TABLE V. Different fits to G_M in physical region. Values of the magnetic form factor G_M, and statistical errors ΔG_M for the polynomial fits of Table IV.

		Free cubic		Constrained quartic		Constrained and restricted quintic	
η	$t(\text{F}^{-2})$	G_M	ΔG_M	G_M	ΔG_M	G_M	ΔG_M
0.960	2.00	1.125	0.395	3.438	0.109	2.636	0.218
0.88	1.97	1.838	0.299	3.444	0.101	2.729	0.197
0.80	1.90	2.372	0.219	3.442	0.088	2.860	0.165
0.72	1.79	2.745	0.154	3.420	0.072	2.986	0.128
0.64	1.61	2.972	0.102	3.368	0.054	3.074	0.092
0.56	1.26	3.070	0.062	3.278	0.037	3.103	0.059
0.48	1.01	3.055	0.032	3.147	0.021	3.061	0.032
0.40	0.53	2.946	0.011	2.972	0.008	2.944	0.012
0.333	0.00	2.793	0.000	2.793	0.000	2.793	0.000
0.320	−0.12	2.757	0.002	2.754	0.001	2.757	0.002
0.200	−1.56	2.362	0.011	2.354	0.010	2.365	0.011
0.080	−3.78	1.883	0.012	1.887	0.012	1.882	0.012
−0.040	−7.38	1.376	0.011	1.388	0.011	1.370	0.011
−0.160	−13.2	0.898	0.010	0.907	0.010	0.892	0.011
−0.280	−23.3	0.504	0.008	0.503	0.008	0.505	0.008
−0.400	−41.5	0.251	0.010	0.254	0.011	0.249	0.010
−0.520	−78.1	0.195	0.037	0.245	0.043	0.137	0.032
−0.640	−180	0.392	0.085	0.579	0.108	0.149	0.073
−0.760	−427	0.898	0.158	1.370	0.216	0.215	0.148
−0.880	−1958	1.769	0.260	2.746	0.383	0.213	0.290
−1.000	$-\infty$	3.062	0.398	4.847	0.623	−0.045	0.545

Table III illustrates the dangers of introducing more adjustable parameters than are needed to fit the data with a value of ϕ near unity. The constrained quartic fit ($N=4$) already has appreciable errors in the coefficients a_n, particularly for large n. (For brevity we give here only the noncorrelated errors rather than the entire error matrix.) The errors are about 1% for small n, and about 10% for large n. For a constrained quintic fit to the data, the errors for small n increase by about a factor of 2 compared to the constrained quartic, while the errors for large n become quite large. The values of a_0 and a_1 change very little, and the errors in them remain small, even when we increase N to 6, since a_0 and a_1 are determined quite accurately by the data in the region $|\eta|<0.1$.

Table IV gives the coefficients for different polynomial fits to the magnetic form factor, for a free cubic, a constrained quartic, and a constrained and restricted quintic. Again we give only the diagonal errors. We observe again that a_0 and a_1 are quite accurately determined, and are practically unchanged from one fit to another. The value of a_N is determined to relatively poor accuracy—namely about $\frac{1}{2}$, or 10% of its value.

The sets of values of a_n given in Table IV are used first to give the (real) form factor for real η, and then to give the imaginary part of the form factor at the cut; i.e., the spectral function.

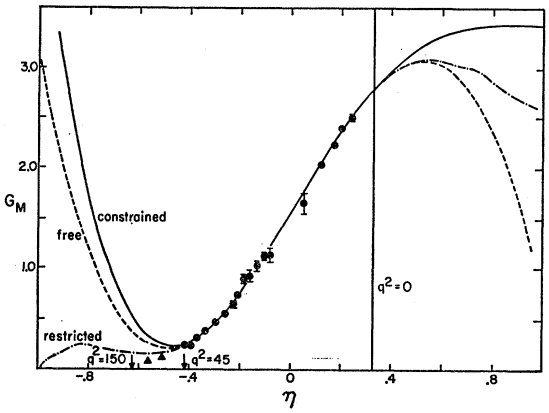

FIG. 4. Fits to the magnetic form factor of the proton, for real η. The points with errors show the data of Table I; the dashed curve is the free-cubic fit; the solid curve is the constrained-quartic fit; and the dash-dot curve is the restricted- and constrained-quintic fit. See Table IV. The triangles represent new data not used in the fit.

Table V gives the form factor $K_M(\eta)$ for real η for the three different polynomial fits of Table IV. The errors in $K_M(\eta)$ are found using the complete error matrix. Thus, there is no error for the static form factor ($\eta=\frac{1}{3}$) since the static magnetic moment has been used as a constraint. In the region $-0.4\leq\eta\leq0.333$, where there are accurate experimental data, all three fits have small errors (of order 0.01) and agree with each other within these small errors. Of course, this must be the case, since all three fits have acceptable values of χ^2. The three fits each show much larger errors, and disagree greatly (many standard errors of the difference) as we extrapolate either towards $\eta=1$ ($t=t_0$, in the nonphysical region) or towards $\eta=-1$ ($t=-\infty$). These results are also presented in Fig. 4, where we show as circles the data of Table I, and as triangles two new Cambridge Electron Accelerator (CEA) points.[12]

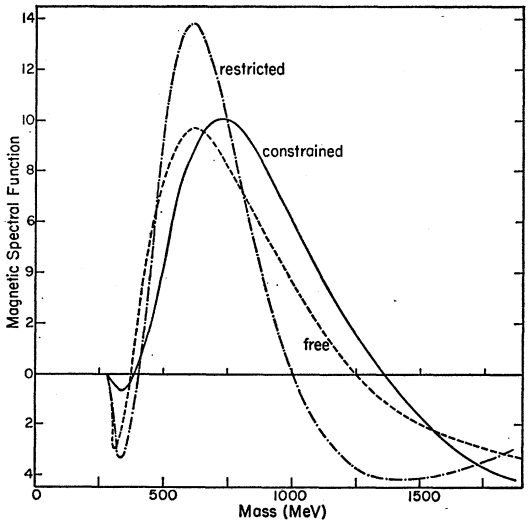

FIG. 5. Spectral function for the proton magnetic form factor, versus mass of the intermediate state in MeV. The dashed curve is the free-cubic fit; the solid curve is the constrained-quartic fit; the dash-dot curve is the constrained- and restricted-quintic fit. See Table VI.

TABLE VI. G_M spectral functions. The spectral function is found using the coefficients a_n from Table IV for three different fits to the magnetic form factor. The mass is $280\,t^{1/2}$; the angle ξ is found from t by Eq. (4), for $b=2$.

		Free cubic		Constrained quartic		Constrained and restricted quintic	
ξ (deg)	Mass (MeV)	$g(t)$	Error	$g(t)$	Error	$g(t)$	Error
0	280	0	0	0.	0	0	0
14.1	289	−2.48	0.32	−0.09	0.02	−0.46	0.08
25.8	308	−3.18	0.46	−0.41	0.12	−1.97	0.35
37.3	337	−2.16	0.44	−0.70	0.26	−3.43	0.65
47.5	373	0.18	0.29	−0.41	0.37	−2.75	0.68
58.1	418	3.32	0.09	0.88	0.36	0.90	0.35
66.1	459	5.79	0.19	2.64	0.26	5.27	0.35
74.6	509	7.96	0.36	4.99	0.10	9.93	0.82
83.3	571	9.37	0.49	7.53	0.27	13.2	1.1
89.9	622	9.66	0.52	8.98	0.45	13.8	1.1
96.1	683	9.29	0.51	9.90	0.59	12.6	0.95
100	718	8.84	0.48	10.07	0.64	11.3	0.78
104	757	8.21	0.43	9.99	0.67	9.62	0.61
106	800	7.41	0.38	9.64	0.67	7.66	0.48
114	903	5.36	0.23	8.08	0.58	3.26	0.57
122	1037	2.91	0.10	5.41	0.38	−0.82	0.83
126	1120	1.63	0.11	3.76	0.25	−2.38	0.89
129	1217	0.38	0.18	1.99	0.13	−3.47	0.88
134	1333	−0.78	0.26	0.20	0.16	−4.05	0.80
138	1474	−1.81	0.32	−1.52	0.30	−4.11	0.66
142	1647	−2.65	0.38	−3.05	0.43	−3.72	0.51
147	1867	−3.27	0.41	−4.28	0.54	−2.99	0.40
155	2545	−3.70	0.41	−5.52	0.65	−1.16	0.50
164	4000	−3.03	0.32	−4.82	0.55	0.18	0.56
174	9333	−1.48	0.15	−2.43	0.27	0.39	0.32
180	∞	0	0	0	0	0	0

Table VI and Figs. 5 and 6 show the extrapolations to the unit circle, to determine the spectral function. Again, the complete error matrix has been used. We present the spectral functions both versus the mass of the intermediate state, $280t^{1/2}$ MeV, and versus the angle ξ. The free cubic spectral function (dashed line) first dips sharply, then has a broad peak around 600 MeV, and becomes negative again at 1250 MeV. The constrained quartic (solid line) has only a small dip near threshold. Again we see a marked but broad peak, this time at 750 MeV. The spectral function becomes negative at 1350 MeV. The restricted and constrained quintic (dash-dot line) shows a dip somewhat above threshold (angle ξ about 40°) and a peak at 620 MeV. This peak is the narrowest of the three, with full width at half-maximum of 300 MeV. The spectral function becomes negative at 1000 MeV.

We see that the same general feature of a strong peak around 650 MeV and a negative spectral function above some 1200 MeV persists in all three fits to the magnetic form factor. In terms of the angle ξ, the peak is centered near 90°, and has a width decreasing from 55° for the free cubic to 40° for the constrained and restricted quintic.

We adopt the same procedures in fitting the data for

TABLE VII. Data used for G_E.

$q^2=-t$	η	G_E	Error	Ref.
0.30	0.302	0.970	0.004	a, b
0.49	0.284	0.932	0.009	b
0.60	0.274	0.940	0.006	a
1.00	0.240	0.885	0.005	a, b
1.05	0.237	0.884	0.009	c
1.60	0.197	0.850	0.010	a
2.00	0.171	0.784	0.012	b
2.20	0.160	0.790	0.006	a
2.98	0.118	0.725	0.022	c
4.0	0.072	0.696	0.032	d
6.0	0.000	0.526	0.021	e
10.0	−0.101	0.414	0.020	d, e, f
14.0	−0.173	0.365	0.027	e
18.0	−0.226	0.310	0.026	e
25	−0.295	0.396	0.037	g
30	−0.333	0.359	0.037	g
35	−0.366	0.258	0.044	g
40	−0.393	0.436	0.073	g
45	−0.416	0.000	0.255	g

[a] D. J. Drickey and L. N. Hand, Phys. Rev. Letters **9**, 521 (1962).
[b] B. Dudelzak, G. Sauvage, and P. Lehmann, Nuovo Cimento **28**, 18 (1963).
[c] P. Lehmann, R. Taylor, and R. Wilson, Phys. Rev. **126**, 1183 (1962).
[d] K. Berkelman, M. Feldman, and G. Rouse, Phys. Letters **6**, 116 (1963).
[e] J. R. Dunning, Jr., K. W. Chen, N. F. Ramsey, J. R. Rees, W. Shaler *et al.*, Phys. Rev. Letters **10**, 500 (1963).
[f] T. J. Janssens, R. Hofstadter, E. B. Hughes, and M. R. Yearian, Bull. Am. Phys. Soc. **7**, 620 (1962).
[g] K. Berkelman, M. Feldman, R. M. Littauer, G. Rouse, and R. R. Wilson, Phys. Rev. **130**, 2061 (1963).

the electric form factor, except that we have not made a restricted fit. Table VIII gives the coefficients a_n, and their errors, for a constrained quartic fit to the data of Table VII. The constrained quartic fit has a χ^2 value of 28.9 for 16 deg of freedom, as compared to a χ^2 value of 61.9 for a constrained cubic fit, and a χ^2 value of 28.4 for a constrained quintic fit. The data on G_E thus has sufficient range and accuracy to need a fit with 3 adjustable parameters, as was the case for the G_M data of Table I. The large χ^2 value for the constrained quartic can be ascribed partly to the disagreements among different laboratories in the measurements, particularly in the range $14 \leq q^2 \leq 25\text{F}^{-2}$, and partly to imposing the static limit $G_E(0)=1.000$ as known precisely. We assumed that there were no systematic errors in the data not included in the quoted standard errors.

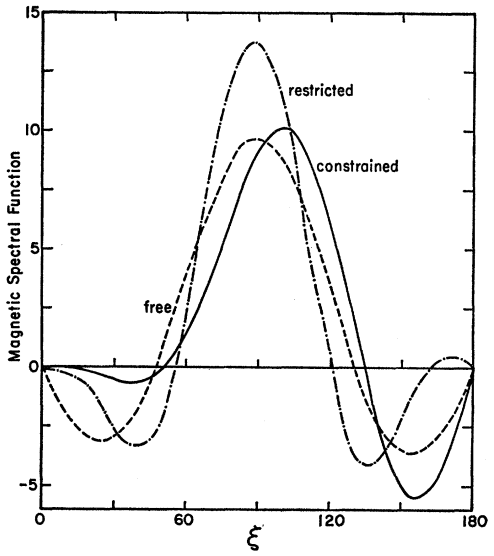

FIG. 6. Spectral function for the proton magnetic form factor, versus angle ξ. The dashed curve is the free-cubic fit; the solid curve is the constrained-quartic fit; the dash-dot curve is the constrained- and restricted-quintic fit. See Table IV.

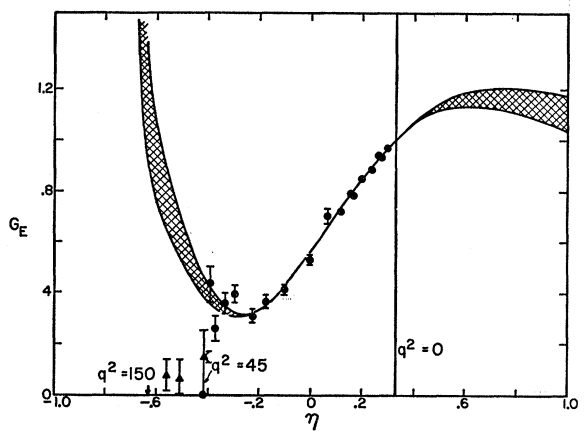

FIG. 7. Fit to the electric form factor of the proton, for real η. The circles show the data of Table VII; the constrained-quartic fit has coefficients shown in Table VIII. The shaded region shows the statistical error of the extrapolation. The triangles represent new data not used in the fit.

Figure 7 gives the values found for the electric form factor $K_E(\eta)$, using the coefficients of Table VIII. The spread of the curve shows the standard error, found using the error matrix of the coefficients. As in the magnetic form factor fit, the error is small (less than 0.02) in the region where there are good data points, but rapidly becomes large in the region $\eta \leq -0.3$ ($q^2 \geq 25$) where the data are either inaccurate, or nonexistent. The subtraction constant, given by the fit $G_E(-\infty)=5.28\pm0.83$ seems unreasonably large: See the discussion above of restricted fits to G_M. The triangles show the new CEA data[12] not used in the fits.

Figure 8 gives the spectral function for the electric form factor, using the coefficients of Table VIII. We also show the spread in the curve. The spectral function of G_E is quite similar to that for the constrained quartic fit to G_M shown in Fig. 5. That is, we see first a small

TABLE VIII. Coefficients for fit to G_E. The coefficients a_n and errors Δa_n for constrained quartic fit to the G_E data of Table VII.

n	a_n	Δa_n
0	0.554	0.008
1	1.393	0.047
2	0.784	0.096
3	−3.473	0.487
4	1.864	0.325

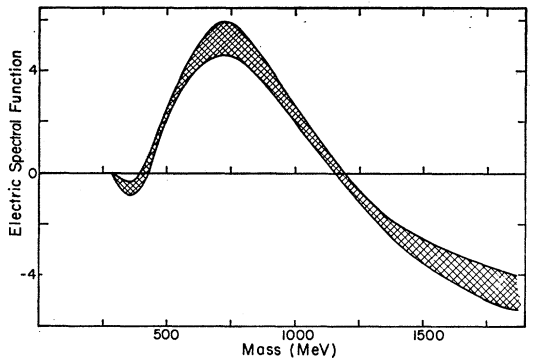

FIG. 8. Spectral function for the electric form factor of the proton versus the mass of the intermediate state in MeV. The constrained-quartic fit has statistical errors given by the shaded region. See Table VIII.

negative dip near threshold, of dubious statistical significance. We then see a marked peak at about 700 MeV, with a width of 470 MeV. The spectral function goes negative near 1200 MeV.

The experiment[13] on proton-antiproton annihilation into an electron-positron pair gives preliminary results for the total cross section for 2.5 BeV/c antiprotons, which is proportional to

$$G^2=|G_E|^2-(q^2/2M^2)|G_M|^2. \tag{11}$$

At this antiproton energy, $q^2=-175\text{F}^{-2}$, and $-q^2/2M^2=3.9$, where M is the nucleon mass.

For a form factor G_E, we have from Eqs. (3) to (5) for real coefficients a_n

$$|G_E|^2=|\sum_{n=0}^{N} a_n \exp(in\xi)|^2$$
$$=\sum_{n=0}^{N} a_n^2+\sum_{n<m} 2a_n a_m \cos(n-m)\xi. \tag{12}$$

Our constrained but nonrestricted fits to G_E and G_M, given in Tables VIII and IV, respectively, give by substitution in Eqs. (11) and (12)

$$G^2=27+130=157,$$

where the first term is $|G_E|^2$. If we use our *restricted* G_M fit of Table IV, the second term is reduced dramatically from 130 to 16. We have not calculated the statistical errors in these values of G^2.

Since the preliminary annihilation experimental result is G^2 of order 5, there is further experimental support (i.e., besides the recent CEA experiments) for restricted fits to both electric and magnetic form factors.

[*Note added in proof.* One of us (J.S.L.) and C. P. Wang have made restricted fits to form factor data of April 1964. The spectral functions are quite similar to the restricted fit of Fig. 5; and we find agreement with the preliminary experimental value of G^2.]

TABLE IX. Influence of range and accuracy of data. Fits to artificial data of Clementel-Villi form. All use $b=1$, and fit data from $\eta_{\min}$ to $\eta_{\max}$ with a free or constrained polynomial of degree N.

$\eta_{\min}$	$\eta_{\max}$	Accuracy	Type	N	χ^2	ϕ[b]
−0.658	−0.101	Exp[a]	Constrained	4	19.9	1.24
−0.80	−0.04	1%	Constrained	5	16.0	1.00
−0.6	+0.28	0.1%	Free	5	17.2	0.95
−0.6	0.6	0.1%	Free	6	27.4	1.10
−0.6	0.6	0.1%	Constrained	6	29.0	1.12
−0.92	0.6	0.1%	Free	7	53.1	1.67
−0.92	0.92	0.1%	Constrained	8	80.9	2.02
−0.92	0.92	0.1%	Free	10	46.0	1.24

[a] The values of η and the accuracy are the same as for current experimental measurements of G_M, in Table I.
[b] $\phi=\chi^2$/degrees of freedom.

IV. TESTS WITH ARTIFICIAL DATA

In this section we test the extrapolation procedure used above for determining spectral functions by applying the procedure to artificial data based on assumed spectral functions. We use 3 different types of spectral functions: (i) a single pole, giving a Clementel-Villi form factor; (ii) two moderately narrow resonances; (iii) a single very broad peak.

In each case, after assuming the input spectral function $g_i(t)$, we determine the corresponding form factor $G(t)$, using an unsubtracted dispersion relation. $G(t)$ is evaluated for 20 or more points in a specified range of the variable t, and is converted into "pseudo data" by adding random errors, of Gaussian distribution and predetermined rms value, to each point. We then choose value for b for the conformal transformation, fit with polynomials (free or constrained) in η and extrapolate to the semicircle to find the output spectral function $g(t)$ with statistical errors Δg.

Let us first examine how the degree N of the polynomial in η depends on the range and accuracy of the artificial data. We use a delta function at $7.02t_0$ for the input spectral function, and choose $b=1$. The range of the data in the η plane is given in the first two columns of Table IX, and the rms percentage error is given in the third column. We fit both with free and constrained polynomials, and make an analysis in each case of the χ^2 value against the degree of the polynomial to determine what value of N to use. (See Table II and the related discussion in Sec. III. This procedure of determining N is followed throughout this section.) The values of N, the corresponding χ^2, and $\phi=\chi^2$/degrees of freedom are given in the last three columns. We see that reasonable fits are achieved (ϕ near unity) in all cases except the constrained octic in the next to the last row.

The data of the first row have a range and percentage accuracy corresponding to the data for G_M given in Table I. It is of interest to note that both the data of Table I and of this row of Table IX are fitted with a constrained quartic; i.e., this range and accuracy of data contains enough information to determine 3 adjustable parameters. The second row gives the range of η for values of momentum transfer attainable by the Cam-

TABLE X. Coefficients for fits to Clementel-Villi forms. a_n' is the exact coefficient found from the assumed spectral function. The values of a_n and Δa_n for the constrained quartic are for data of range and accuracy given by the first row of Table IX. The free decic fit is for data of range and accuracy given in the last row of Table IX.

		Constrained quartic		Free decic	
n	a_n'	a_n	Δa_n	a_n	Δa_n
0	1.000	1.000	0.000	1.000	0.000
1	0.570	0.544	0.062	0.572	0.002
2	−0.815	−1.166	0.265	−0.797	0.006
3	0.596	−0.030	0.142	0.611	0.029
4	−0.037	0.469	0.249	−0.249	0.051
5	−0.543	···	···	−0.758	0.117
6	0.814	···	···	1.659	0.165
7	−0.621	···	···	−0.031	0.183
8	0.074	···	···	−1.496	0.229
9	0.515	···	···	0.193	0.097
10	−0.810	···	···	0.468	0.115

bridge Electron Accelerator, and also assumes improved accuracy of 1%. This large increase in range and accuracy gives only one additional parameter. In the last row of the table we examine data extending to extremely large negative values of t, and also far into the nonphysical region, with 0.1% accuracy. These data determine 10 adjustable parameters. The main increase in N comes from increasing the range of the data.

In Table X we give the coefficients a_n, and diagonal errors Δa_n for the constrained quartic and free decic fits (first and last rows of Table IX). It is of interest to compare these coefficients with each other, and also with the coefficients a_n' calculated from the input spectral function. Namely,

$$a_n' = 2(\tan\xi_R + \csc\xi_R)\sin n\xi_R. \tag{13}$$

Here t_R and ξ_R are the positions of the pole, related by Eq. (4). For our choice $t_R = 7.02t_0$, and $b=1$, the angle ξ_R is 135.6°. The assumed delta function in t gives a delta function in ξ, which clearly has Fourier coefficients proportional to $\sin n\xi_R$, as given above. The factors come from changing variables from t to ξ. We see that for low values of n there is good agreement between a_n for the output spectral function and a_n' for the input spectral function. However, the agreement becomes poor for the decic fit for $6 \leq n \leq 10$.

Figures 9(a) and (b) show the spectral functions plotted against angle ξ for the coefficients given in Table X. The input spectral function is a delta function, at angle $\xi_R = 135.6°$, shown in the figure as a vertical line. In Fig. 9(a) the solid curve shows a Fourier series with exact coefficients a_n', truncated at $N=4$, while the dashed line shows the constrained quartic fit to the pseudodata with coefficients a_n. We see that each curve has a broad peak in the general region of the input delta function. There are spurious peaks at other angles, and these spurious peaks are stronger for the constrained quartic fit. In Fig. 9(b) we see that the solid curve for a Fourier series with 10 terms, using the exact

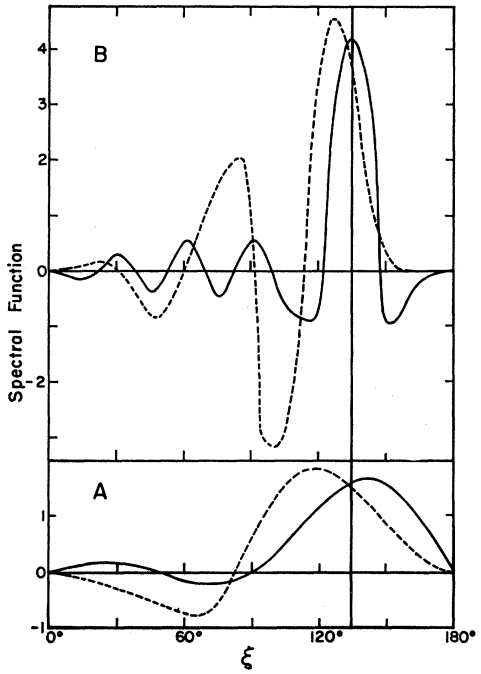

FIG. 9. Spectral functions for one-pole pseudodata versus angle ξ. The input delta function is shown by the vertical line near 135°. The solid curve in 9(a) shows the exact Fourier series truncated at 4 terms; the dashed curve shows the constrained quartic fit. The solid curve in 9(b) shows the exact Fourier series truncated at 10 terms; the dashed curve shows the free-decic fit. See Table X.

coefficients a_n' does give a rather narrow peak centered at the input delta function. The free decic also gives a narrow peak at a somewhat smaller angle. The spurious peaks are quite marked for the free decic fit.

All the above results can be interpreted in terms of the behavior of truncated Fourier series. First, the main peak becomes higher and narrower as we take more terms in the series, the width of the peak decreasing like $180/N$. Second, the spurious peaks are less prominent if we use the exact coefficients a_n', since we then have destructive interference of the terms of the Fourier series. If we introduce errors, giving coefficients a_n, the destructive interference is in general less effective, and the spurious peaks become more prominent. Third, there is a tendency for the coefficients a_n to give a peak shifted from the input value towards 90°. This tendency is exemplified by another treatment of the one-pole artificial data.

TABLE XI. Single-pole positions and strengths. The pole position of the input spectral function is given by Eq. (1.5) for resonance energy $t_R = 7.018t_0$.

b	Input peaks at	Output peaks at
1	135.6°	127°
2	101.6°	96°
5	52.3°	69°

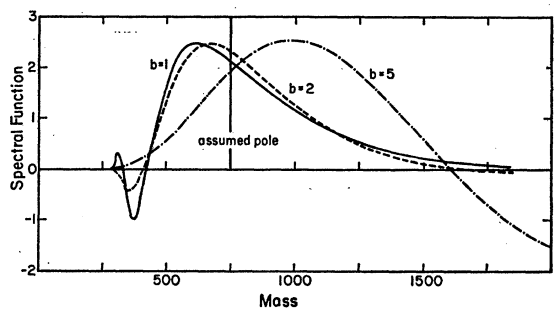

FIG. 10. Spectral functions for constrained-quintic fits to one-pole pseudodata versus mass of the intermediate state, for three choices of the parameter b. The solid curve is for $b=1$; the dashed curve for $b=2$, and the dot-dash curve for $b=5$. The vertical line shows the input delta function at 750 MeV. See Table XI.

We now treat one-pole data, of range and accuracy given by the second row of Table IX, and examine the dependence of the output spectral function on the value chosen for the parameter b. The case $b=1$ gives a constrained quintic, as shown in Table IX. Choosing $b=2$ or $b=5$ also gives constrained quintic fits. Table XI shows that as we vary b over this range, the angular position of the input delta function shifts from 135.6° to 52.3°. The output spectral function has a main peak that shifts position over a somewhat smaller range: namely from 127° for $b=1$ to 69° for $b=5$. In all 3 cases here, as in two other cases for $b=1$ discussed above, the output spectral function tends to have its peak shifted towards 90°. We believe that this effect is due to the tendency of truncated Fourier series to produce a peak near 90°, and the difficulty that a truncated Fourier series has in producing a peak either near 0° or near 180°. For instance, to produce a peak near 180° and a zero at 180° the spectral function would have to fall very rapidly from the peak to the zero. But it is hard for the truncated series to fall very rapidly; therefore it is likely that the peak is shifted away from 180°, and towards 90°.

Figure 10 shows the three spectral functions determined for different choices of b plotted against energy. The input delta function at 750 MeV is shown as a vertical line. The three constrained quintic fits to the same artificial data, using three different values of b, each give broad peaks in the general region of 750 MeV. The solid line for $b=1$ peaks at 620 MeV, the dashed line for $b=2$ peaks at 680 MeV, and the dash-dot line for $b=5$ peaks at 1000 MeV. Of course, these shifts in the energy position of the peak correspond exactly to the shift of angle towards 90° discussed above. The width of the peaks shown in Fig. 10 is in general agreement with our discussion above for the angular width of a peak for a truncated Fourier series; e.g., a 36° angular width is in fair agreement with the width in energy of 500 MeV, for the solid curve.

We now examine the "resolving power" of our extrapolation procedure. That is, if we assume a spectral function consisting of two narrow peaks, how well separated should the peaks be so that the output spectral function will also show two peaks? Figure 11(a) shows as a solid line the input spectral function for two Lorentzian-shaped peaks of opposite sign located at 750 MeV and at 1000 MeV. (The Lorentzians are modified to vanish and have vanishing slope at threshold t_0.) The artificial data are chosen for the range $-58F^{-2}\leq t\leq 0$, and is assumed to have 1% accuracy. We choose $b=2.34$ to center the data, and fit with a constrained quartic. The output spectral function, shown in Fig. 11(a) as a dashed line, is unsuccessful in resolving the two peaks. However, it does have a feature not generally found in fits to one-pole data; namely, at high energy the output spectral function makes a large negative excursion. The negative peak is centered at 3000 MeV [far beyond the limits of Fig. 11(a)] and has a value of −0.61, compared with the positive peak of 2.0 at 750 MeV. That is, the two input peaks are not resolved, but the output spectral function has a

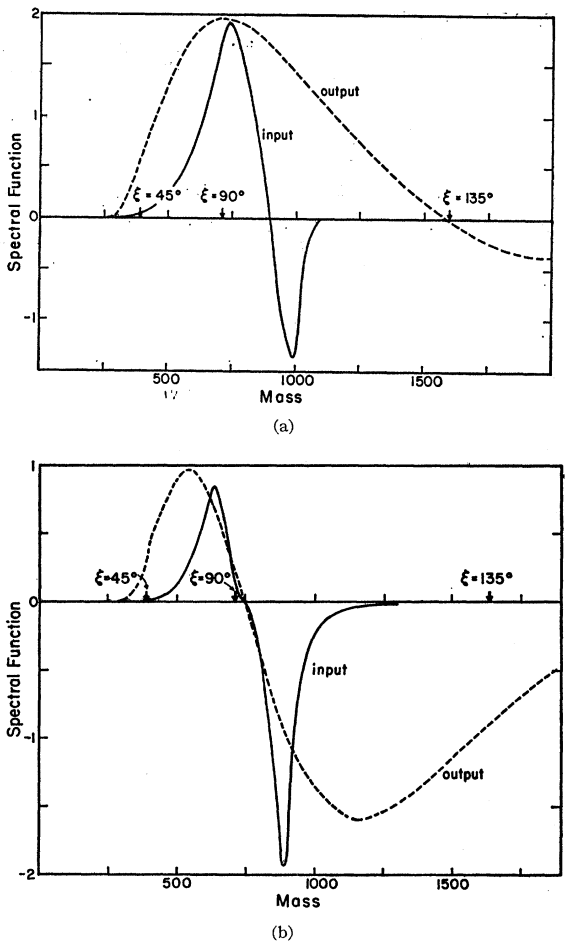

FIG. 11. Two-resonance pseudodata spectral functions versus mass of the intermediate state. In 11(a) the input is the solid line, and the output, or extrapolated fit, is the dashed line. The same notation is used in 11(b) for a different input spectral function.

new feature that suggests the presence of some structure hidden in the main broad peak.

In Fig. 11(b) we plot as a solid line an input spectral function for which the negative peak is more significant than in Fig. 11(a). In this case, the output spectral function is more nearly successful in resolving the two peaks: namely, the output peaks at 550 and 1150 MeV, while the input peaks at 650 and 900 MeV. The output is forced to increase the separation of the two peaks, since a Fourier series with only 4 terms cannot reproduce the very sharp variation with angle needed for two peaks at the input positions.

Finally, we apply our method to data based on the input spectral function shown as curves in Figs. 12(a) and (b). This "smooth spectral function" is chosen to have a peak at 750 MeV, with a width of 840 MeV, and the threshold behavior of zero slope of our constrained polynomial fits. These data are chosen to have the range and accuracy given by the second row in Table IX, and we choose $b=2$. Table XII shows that a constrained

TABLE XII. Coefficients for smooth spectral function. The spectral function is shown in Figs. 12(a) and (b).

	Constrained		Free	
n	a_n	Δa_n	a_n	Δa_n
0	0.714	0.002	0.714	0.002
1	0.968	0.003	0.981	0.005
2	−0.224	0.022	−0.221	0.021
3	−0.349	0.018	−0.455	0.037
4	0.132	0.024	...	...
χ^2	18.6		16.5	
ϕ	1.10		0.97	

quartic or a free cubic give statistically satisfactory fits to the data. (For the one-pole spectral function, data of this range and accuracy demanded one extra parameter; i.e., we fitted with a constrained quintic.) The coefficients given in Table XII are used to give the spectral functions shown in Figs. 12(a) and (b). We see that the dots give output spectral function in very good agreement with the input. The error bars for the dots show the statistical error in the spectral function for the constrained quartic fit; and in general the dots are within one standard error of the input value. The output spectral function for the free cubic is shown as triangles. These triangles give a spurious negative peak just above threshold, and also do not fit the input as well in the peak region. The threshold behavior shows that using a constrained polynomial is worthwhile in this case. The behavior of the cubic in the peak region is due to the difficulty of fitting the peak with only 3 terms in the Fourier series. Use of a constrained polynomial allows the determination of a fourth term in a Fourier series, with a constraint for the coefficients, thus permitting the output spectral function to have a narrower peak.

It is of interest to examine all the above artificial data

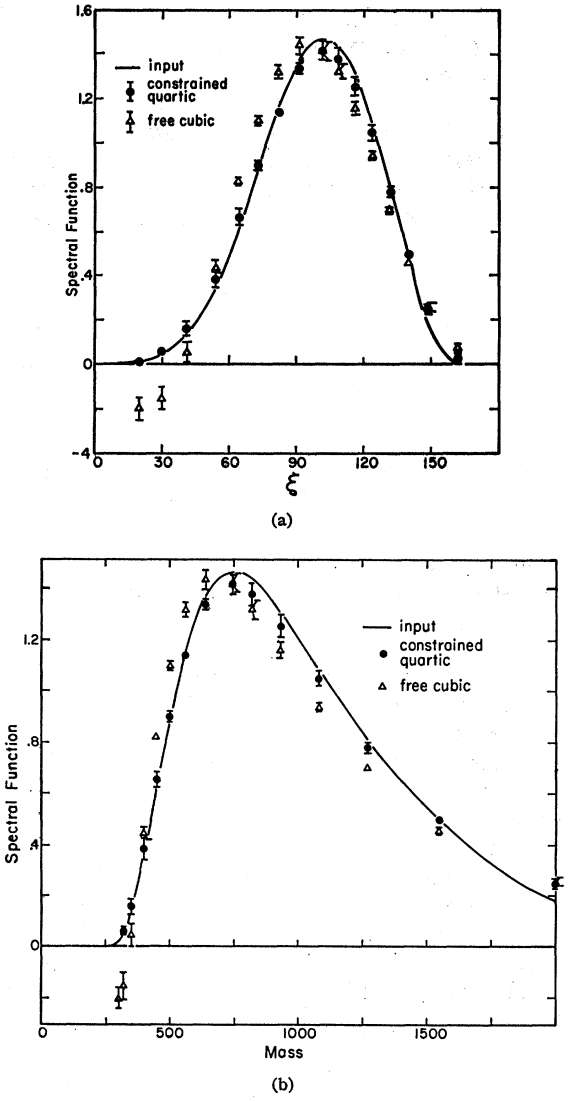

FIG. 12. Smooth spectral function. The input is the solid curve; the output constrained-quartic fit is given by circles with statistical errors, and the output free cubic is given by triangles. 12(a) is a plot of spectral function versus angle ξ; 12(b) is a plot versus mass of the intermediate state. See Table XII.

again, from the opposite point of view: namely, can we achieve a statistically successful fit of the Clementel-Villi form? For the first case of artificial data based on a one-pole spectral function, it is clear that the Clementel-Villi fit must succeed. In particular, if we use the lowest accuracy and lowest range data as given in the first row of Table IX, we find a statistically acceptable value of $\chi^2=21.6$ for 18 deg of freedom. The output position of the pole is $t/t_0=6.9\pm0.12$, in good agreement with the input value of 7.02.

If we use the spectral function of Fig. 11(a) ,which is dominated by a fairly broad resonance at $t/t_0=7$, we find that we can fit with a single pole at $4.9t_0$. The χ^2 value of 18 for 19 deg of freedom is excellent by statisti-

cal criteria, but is slightly larger than the value of 14.5 for 17 deg of freedom, for the constrained quartic fit in η given above.

On the other hand, consider the two-resonance artificial data for the spectral function shown in Fig. 11(b). Here the resonance at higher energy is relatively stronger than in Fig. 11(a), so that our fits by conformal transformation almost succeed in resolving the two peaks. Also with our value of b, the spectral function goes through zero for ξ near 90°, which is not difficult to reproduce with a truncated Fourier series. When we try to fit the data with a Clementel-Villi form, we immediately fail, since the pseudodata $G(t)$ are not monotonic in the physical region: $G(0)$ is adjusted to be exactly unity, while $G(-3t_0)=1.27$; for more negative t, G falls monotonically with increasing $|t|$.

Finally, we attempt a one-pole fit to artificial data based on our smooth spectral function of Fig. 12. This fit is unsuccessful for the range and accuracy chosen for the data giving $\chi^2=187$, but would be statistically acceptable for data of the same range but about 5% accuracy, instead of the 1% accuracy assumed above.

V. CONCLUSIONS

We now wish to ask what the results of Sec. III allow us to deduce about the behavior of the proton form-factor spectral functions $g_M(t)$ and $g_E(t)$. In particular, we wish to know what significance we should attach to the apparent peak below 1 BeV, how confident we can be about its position and width, and how seriously we should take the change of sign seen above 1 BeV. These questions are best considered in the light of experience with pseudodata as discussed in Sec. IV. We should emphasize that the particular examples quoted in Sec. IV and referred to here are merely offered as examples of the behavior of various types of pseudodata. Our conclusions are in many cases based on a variety of such examples showing the same qualitative behavior. In discussing the treatment of actual data in Sec. III, we shall in general refer only to the magnetic form factor; the behavior of the electric form factor is qualitatively the same.

The first question is whether the peak seen in Figs. 5 and 6 is significant. Let us phrase the question in another way, since $g(t)$ vanishes at $t=t_0$ and $t=\infty$ by construction and thus any spectral function will have a maximum somewhere. We wish to ask: Supposing the spectral function were everywhere positive and consisted of a single very broad peak, would an extrapolation of the type carried out in Sec. III be likely to yield results of the type shown in Figs. 5 and 6? Examination of Fig. 12 suggests that this is unlikely—that such a spectral function would be fairly accurately reproduced. The good agreement between input and output in Fig. 12 is perhaps a bit misleading, since the function is well approximated just by $\sin\xi$. However, it is in fact true that the peak in Fig. 6 also lies near $\frac{1}{2}\pi$ and it seems unlikely that all three curves shown would produce a spuriously narrow peak in the same manner. We therefore conclude that the data require a large contribution to the form factor from a relatively localized region of the spectral function.

If we assume that there is, in fact, a relatively sharp, dominant peak, we can then consider its location. Experience with attempted extrapolations of one-pole pseudodata indicate that such peaks obtained by extrapolation are displaced from their "true" positions as functions of ξ towards $\frac{1}{2}\pi$. However, in this case the observed positions are at or near $\frac{1}{2}\pi$ (because of our choice of b, although the reason for this choice was quite different) and so are probably near to their true value. Of the three fits shown in Figs. 5 and 6, probably the constrained and restricted *quintic* is most plausible. In discussing the position we must also take account of the width. A wide peak will behave like a δ function at a position below its maximum. It seems clear that an extrapolation with so few terms can only give an upper limit for the width as seen in the fits of one pole pseudodata. Bearing these points in mind we deduce from our results that there exists a peak of unknown width (less than that of 350 MeV shown in the extrapolation) and position about 625 MeV ($\xi=\frac{1}{2}\pi$) with a considerable uncertainty (of the order of 150 MeV). This position is in quite reasonable agreement with the $\rho-\omega$ mixture assumed in fact to dominate $g_M{}^p$.

As regards the negative excursion above 1 BeV, it seems likely that it is a significant effect. It is true that a similar behavior is obtained in Fig. 10 when a single δ function is fitted at about the same mass as the ρ meson with $b=5$. However, in this case, the position of the pole corresponds to $\xi=69°$. In order for a positive peak to occur at all at such a low angle the dominant term has to be $\sin 2\xi$, and this causes the negative excursion in Fig. 10. As pointed out above, the experimental data indicate a peak at $\frac{1}{2}\pi$ which would need no even terms at all, in principle, and in fact they are small. Furthermore, even in the example where a quintic fit to a pole at the ρ mass does introduce a spurious negative excursion it occurs at an energy appreciably higher than in the quintic fit to the experimental data.

We cannot make any strong statements about the structure of this negative component. If we identify the main peak with the ρ and ω mesons, it is possible to speculate whether the ϕ is responsible for the higher mass negative component. The results shown in Fig. 11(a) based on a spectral function representing roughly the $\rho-\omega$ and ϕ contributions are quite similar to the constrained quartic fit achieved for the experimental data.

The conclusions we can draw about the spectral function are essentially the same as those obtained by the two-pole fits to the data discussed in the Introduction. The dominance of a peak near the $\rho-\omega$ mass and the change in sign of the spectral function above 1 BeV, consistent with an appreciable contribution from the ϕ meson. We have therefore gained no new information

by using the full analytic properties of G. However, this information has been gained without at any stage having to insert any external assumptions about the nature of the spectral function, such as the position of the $\rho-\omega$ peak; we are led directly by the data and our extrapolation procedure to infer a low-energy positive contribution and a higher energy negative one.

Clearly, with better measurements we should be able to say more about the spectral function. From the discussion of Sec. IV it is clear that increased range is much more important than increased accuracy: The former allows more coefficients to be determined, while the latter merely increases the accuracy with which the same number can be determined. Increased range is being provided by measurements at the Cambridge Electron Accelerator,[12] and by measurements[13] of proton-antiproton annihilation to electron-positron pairs. It would be possible to express the cross sections directly as power series in η and fit them by this method instead of first deducing form factors. This should improve the accuracy of the fits; as indicated above this in itself will probably not shed much more light on the spectral function, but it does mean that measurements can then be incorporated for values of t at which there are not enough data to determine the form factors with any accuracy. Of course it would be of interest to examine the isoscalar and isovector spectral functions separately, as improved neutron data become available.

ACKNOWLEDGMENT

We are grateful to many members of the Laboratory of Nuclear Studies for helpful discussions of our work. We also wish to thank M. W. Kirson for allowing us to use his results on two-pole fits; and we wish to thank C. Lovelace, R. Theis, and J. D. L. Zeiler for informing us of their work in the η plane. Our numerical work was done on the 1604 computer at Cornell.

APPENDIX: LEAST-SQUARES FITS WITH CONSTRAINTS

We give first a summary of the usual theory of statistical curve fitting.[14] Suppose we make m measurements of some quantity y which is a function $f(x; a_1,\cdots a_N)$ of one variable x and N parameters a_r. The measurements y_i are made at points x_i subject to experimental errors z_i. Let $\rho(a_1,\cdots a_N; x_i,y_i,z_i)$ be the probability of observing the value y_i at the point x_i, if the experimental error is z_i and the values of the parameters are $a_1\cdots a_N$. Assuming the observations to be independent, the combined probability that the actual observations should have occurred depends on the values $a_1\cdots a_N$ and the x_i, y_i, z_i

$$P(a_1\cdots a_N)=\prod_{i=1}^{m}\rho(a_1\cdots a_N; x_i; y_i; z_i). \quad \text{(A1)}$$

We define

$$M=-\ln P=-\sum_{i=1}^{m}\ln\rho(a_1\cdots a_N; x_i; y_i; z_i), \quad \text{(A2)}$$

whose minimum gives the maximum value of P. We find this minimum by setting

$$\partial M/\partial a_r=0, \quad r=1,\cdots N, \quad \text{(A3)}$$

and let a_r^0 be the values of a_r for which (A3) are satisfied. These are then the best values of the parameters a_r, and the best interpolation or extrapolation for the function f is $f(x,a_1^0\cdots a_N^0)$. In order to estimate the error on this extrapolation we expand M about the point a_r^0; setting $a_r=a_r^0+\Delta a_r$: to the lowest order

$$M=M^0+\sum_{rs}\left(\frac{\partial^2 M}{\partial a_r\partial a_s}\right)^0\Delta a_r\Delta a_s, \quad \text{(A4)}$$

where the superscript 0 indicates the value at the maximum point.

We set $H_{rs}=(\partial^2 M/\partial a_r\partial a_s)^0$; $\mathbf{H}$ is therefore a symmetric numerical matrix calculated from the experimental observations. Hence, there must be some orthogonal matrix $\mathbf{D}$ which diagonalizes $\mathbf{H}$

$$\mathbf{DHD}^T=\mathbf{h}, \quad \text{(A5)}$$
$$h_{rs}=h_{rr}\delta_{rs},$$

and we may set $h_{rr}=1/\lambda_r^2$. If we were to choose a new set of parameters

$$b_r=\sum_s D_{rs}a_s \quad \text{(A6)}$$

we would have

$$M=M^0+\sum_r(\Delta b_r/\lambda_r)^2$$

provided we have been justified in neglecting higher terms. We could write

$$P(b_1\cdots b_N)=\text{const}\exp[-\textstyle\sum_r(\Delta b_r/\lambda_r)^2]$$
$$=\text{const}\Pi_r\exp[-(\Delta b_r/\lambda_r)^2]. \quad \text{(A7)}$$

Since P is essentially the combined probability distribution for the b_{r_0}, we conclude that the b_r are independently Gaussian with mean b_r^0 and rms error λ_r. Hence, if $g(b_1\cdots b_N)$ is some quantity depending on the b_r, the error in g corresponding to an error Δb_r is $(\partial g/\partial b_r)\Delta b_r$ and its rms value is

$$(\partial g/\partial b_r)\langle\Delta b_r\rangle=\lambda_r(\partial g/\partial b_r).$$

The over-all rms error in g from its best value $g(b_r^0)$ is

$$\Delta g=\left[\sum_r\left(\lambda_r\frac{\partial g}{\partial b_r}\right)^2\right]^{1/2}=\left[\sum_{rs}\frac{\partial g}{\partial b_r}\lambda_r^2\delta_{rs}\frac{\partial g}{\partial b_s}\right]^{1/2}$$
$$=\left[\sum_{rs}\frac{\partial g}{\partial b_r}h_{rs}^{-1}\frac{\partial g}{\partial b_s}\right]^{1/2}. \quad \text{(A8)}$$

[14] See, for instance, J. Orear, University of California Radiation Laboratory Report No. UCRL-8417, 1958 (unpublished), or M. G. Kendall and A. Stuart, *The Advanced Theory of Statistics* (Hafner Publishing Company, New York, 1961), Vol. 2, Chap. 19.

Now since b and a are linearly related,

$$\partial g/\partial b_r=\sum_t D_{rt}^{-1}(\partial g/\partial a_t).$$

Thus, $g=g(a_r^0)$ with an rms error

$$\langle\Delta g\rangle=\left[\sum_{tu}\frac{\partial g}{\partial a_t}H_{tu}^{-1}\frac{\partial g}{\partial a_u}\right]^{1/2}. \tag{A9}$$

H_{tu}^{-1} is thus the error matrix associated with the parameters a.

We now may ask for a similar determination subject to c constraints.

$$\phi_\alpha(a_1\cdots a_N)=0, \quad \alpha=1\cdots c. \tag{A10}$$

This is easily done using Lagrange multipliers μ by replacing M by M', where

$$M'=M+\sum_{\alpha=1}^{c}\mu_\alpha\phi_\alpha, \tag{A11}$$

and setting

$$\partial M'/\partial a_r=0, \quad \partial M'/\partial\mu_\alpha=0. \tag{A12}$$

Formally, we may regard M' as being the likelihood function associated with the $N+c$ free parameters $a_1\cdots a_N, \mu_1\cdots\mu_c$. Accordingly, all of the above analysis of error can be carried over exactly as before. The matrix $\mathbf{H}$ is an $(N+c)\times(N+c)$ partitioned matrix:

$$\mathbf{H}=\begin{bmatrix}\partial^2M/\partial a_r\partial a_s & \partial\phi_\alpha/\partial a_r\\ \partial\phi_\alpha/\partial a_s & 0\end{bmatrix}. \tag{A13}$$

$r=1,\cdots N$; $s=1,\cdots N$; $\alpha=1\cdots c$. The derivatives are evaluated at the point determined by (A12). From (A9) we see that the error matrix associated with the constrained a's is simply the top $N\times N$ minor of the matrix $\mathbf{H}^{-1}$, since g does not depend explicitly on the μ_α.

The formulation becomes very simple for linear least-squares fits and linear constraints. In this case

$$f(x,a_1\cdots a_N)=\sum_{r=1}^{N}a_rf_r(x) \tag{A14}$$

and if the errors in y are Gaussian,

$$\ln\rho=-[\sum_{r=1}^{N}a_rf_r(x)-y_i]^2/z_i^2. \tag{A15}$$

The constraints are

$$\phi_\alpha=\sum_{r=1}^{N}k_{\alpha r}a_r-d_\alpha=0. \tag{A16}$$

Thus,

$$M'=\sum_{i=1}^{m}\left[\frac{\sum_{r=1}^{N}a_rf_r(x_i)-y_i}{z_i}\right]^2+\sum_{\alpha=1}^{c}\mu_\alpha(\sum_r k_{\alpha r}a_r-d_\alpha);$$

if we define $a_{N+l}=\frac{1}{2}\mu_l$, we can write this compactly as

$$M'=\sum_{r,s=1}^{N+c}H_{rs}a_ra_s-\sum_{r=1}^{N+c}2a_ru_r+Y, \tag{A17}$$

where

$$\begin{aligned}H_{rs}&=\begin{bmatrix}\sum_{i=1}^{m}\dfrac{f_r(x_i)f_s(x_i)}{z_i^2} & k_{\alpha r}\\ k_{\alpha s} & 0\end{bmatrix},\\ u_r&=[\sum_{i=1}^{m}f_r(x_i)y_i/z_i^2, \quad d_\alpha],\\ Y&=\sum_{i=1}^{m}(y_i/z_i)^2,\end{aligned} \tag{A18}$$

and the solution to (A12) is

$$a_r^0=\sum_{s=1}^{N+c}(H^{-1})_{rs}u_s, \tag{A19}$$

$\mathbf{H}^{-1}$ being the error matrix. Thus, we see that the only modification necessary to an ordinary linear least-squares fit is a simple extension of the matrix $\mathbf{H}$.